

# Volumetric Segmentation of Multiple Basal Ganglia Structures

Mustafa Gökhan Uzunbaş, Octavian Soldea, Müjdat Çetin,  
Gözde Ünal, Aytül Erçil, and Ahmet Ekin,<sup>\*†‡</sup>

## Abstract

We present a new active contour-based, statistical method for simultaneous volumetric segmentation of multiple subcortical structures in the brain. Neighboring anatomical structures in the human brain exhibit co-dependencies which can aid in segmentation, if properly analyzed and modeled. Motivated by this observation, we formulate the segmentation problem as a maximum *a posteriori* estimation problem, in which we incorporate statistical prior models on the shapes and inter-shape (relative) poses of the structures of interest. This provides a principled mechanism to bring high level information about the shapes and the relationships of anatomical structures into the segmentation problem. For learning the prior densities based on training data, we use a nonparametric multivariate kernel density estimation framework. We combine these priors with data in a variational framework, and develop an active contour-based iterative segmentation algorithm. We test our method on the problem of volumetric segmentation of basal ganglia structures in magnetic resonance (MR) images. We compare our technique with existing methods and demonstrate the improvements it provides in terms of segmentation accuracy.

## 1 Introduction

Magnetic resonance (MR) image segmentation is fundamental in obtaining anatomical and functional information from biological structures and tissues, being used towards visualization, surgical guidance, diagnosis, and quantitative analysis [6]. MR image segmentation provides the location of structures of interest in a non-invasive inspection and, therefore, it is a required step when analyzing the relationships between structural and functional abnormalities, which allows for diagnosis of diseases. For example, segmentation of subcortical structures in brain MR images is motivated by a number of medical objectives including the early diagnosis of neurodegenerative illnesses such

---

\*Gökhan Uzunbaş, Octavian Soldea, Müjdat Çetin, Gözde Ünal, and Aytül Erçil are with the Faculty of Engineering and Natural Sciences, Sabanci University, Istanbul, 34596 Turkey. e-mails: uzunbas@su.sabanciuniv.edu, octavian, mcetin, gozdeunal, aytulerdil@sabanciuniv.edu

†Ahmet Ekin is with the Video Processing and Analysis Group, Philips Research, Europe, Eindhoven, 5656AE, The Netherlands. e-mail: ahmet.ekin@philips.com

‡This work was partially supported by the European Commission under Grants FP6-2004-ACC-SSA-2 (SPICE), MIRG-CT-2006-041919, MTKI-CT-2006-042717, and a graduate fellowship from The Scientific and Technological Research Council of Turkey (TUBITAK).

as schizophrenia, Parkinson’s, and Alzheimer’s diseases. In this context, the analysis of chemicals in Basal Ganglia structures is thought to provide important cues [4], and accurate segmentation is necessary for such an analysis.

Variational techniques provide a principled framework for formulating segmentation problems [1, 8], and have been widely used with biomedical data. In this paper, we introduce statistical joint prior models of multiple-structures into an active contour segmentation method in a nonparametric multivariate kernel density estimation framework. In our previous work [9], we introduced prior probability densities on the coupled (joint) shapes of the structures of interest for 2D segmentation. In this paper, we propose a framework which includes not only coupled shape priors, but also inter-shape (relative) pose priors for the multiple structures to be segmented, and apply this technique to 3D data. We use multivariate Parzen density estimation to estimate the unknown joint density of multiple object shapes, as well as inter-shape poses, based on expert-segmented training data. For inter-shape pose representation, we use standard moments, which are intrinsic to shape and have natural physical interpretations [5]. Given these learned prior densities, we pose the segmentation problem as a maximum *a posteriori* estimation problem combining the prior densities with data. We derive gradient flow expressions for the resulting optimization problem, and solve the problem using active contours. To the best of our knowledge, our approach is the first scheme of multi-object segmentation employing coupled nonparametric shape and inter-shape pose priors.

## 2 Segmentation Using Coupled Priors

We define an energy (cost) functional in a MAP estimation framework as

$$E(\mathbf{C}) = -\log P(\text{data}|\mathbf{C}) - \log P(\mathbf{C}), \quad (1)$$

where  $\mathbf{C}$  is a set of evolving contours  $\{C^1, \dots, C^m\}$  that represent the boundaries of  $m$  different anatomical structures (e.g. caudate nucleus, putamen, etc.). In the following, we will refer to [1] as *C&V*. We choose the likelihood term  $P(\text{data}|\mathbf{C})$  as in *C&V*. In this work, we focus on building  $P(\mathbf{C})$ , which is a coupled prior density of multiple structures (or objects).

The geometric information in  $\mathbf{C}$  consists of shape  $\tilde{\mathbf{C}}$  and pose  $\mathbf{p}$ , i.e.  $P(\mathbf{C}) = P(\tilde{\mathbf{C}}, \mathbf{p})$ , where  $\mathbf{p}$  is a vector of pose parameters (location, size, orientation) for each structure, and  $\tilde{\mathbf{C}} = T[\mathbf{p}]\mathbf{C}$  denotes the aligned version of the boundaries (i.e.  $T[\mathbf{p}]$  is an alignment operator that brings the curves to some reference pose). We decompose the pose  $\mathbf{p}$  into a global pose  $p_{glb}$  of the ensemble of structures, and inter-shape poses  $\mathbf{p}_{int} = (p_{int}^1, \dots, p_{int}^m)$  of each structure, i.e.  $\mathbf{p} = (p_{glb}, \mathbf{p}_{int})$ . When the structures are globally aligned, the remaining variability in the pose of individual structures is captured by  $\mathbf{p}_{int}$ . Given these definitions, we have

$$P(\mathbf{C}) = P(p_{glb}, \mathbf{p}_{int}|\tilde{\mathbf{C}}) \cdot P(\tilde{\mathbf{C}}). \quad (2)$$

Conditioned on  $\tilde{\mathbf{C}}$ , we model  $p_{glb}$  and  $\mathbf{p}_{int}$  as independent variables, because the global pose of the structures and inter-shape poses are not expected to provide information about each other. In addition,  $P(p_{glb}|\tilde{\mathbf{C}})$  is assumed to be uniform since all poses  $p_{glb}$  are equally likely.<sup>1</sup> Then (2) becomes

$$P(\mathbf{C}) = P(\mathbf{p}_{int}|\tilde{\mathbf{C}}) \cdot \gamma \cdot P(\tilde{\mathbf{C}}),$$

---

<sup>1</sup>In some applications where certain global poses are more likely *a priori*, a non-uniform density could be used.

where  $\gamma$  is a normalizing scalar. In this context, the coupled shape density  $P(\tilde{\mathbf{C}})$  disregards all the pose variability and focuses only on shape variability, whereas  $P(\mathbf{p}_{int}|\tilde{\mathbf{C}})$  provides a density on the relative pose of shapes. The inter-shape pose prior is estimated over globally aligned multiple object contours while the shape prior is estimated over both globally and locally aligned ones. Considering this key point, let  $\bar{\mathbf{C}} = (\mathbf{p}_{int}, \tilde{\mathbf{C}})$  denote the globally aligned multiple object contours, (see Figure1). We can then represent the inter-shape pose prior in terms of the curves which encompass internal pose variation, conditioned on the shapes whose global and local pose variation is removed. Then the overall prior can be written as:

$$P(\mathbf{C}) = P(\bar{\mathbf{C}}|\tilde{\mathbf{C}}) \cdot \gamma \cdot P(\tilde{\mathbf{C}}).$$

Using these definitions, (1) can be expressed as

$$E(\mathbf{C}) \propto -\log P(\text{data}|\mathbf{C}) - \log P(\bar{\mathbf{C}}|\tilde{\mathbf{C}}) - \log P(\tilde{\mathbf{C}}). \quad (3)$$

Segmentation is achieved by finding the set of curves  $\mathbf{C}$  that minimize (3) through active contour-based gradient flow.

## 2.1 Coupled Shape Prior for Multiple Structures

In this subsection we discuss the learning and use of  $P(\tilde{\mathbf{C}})$ . We have  $N$  training samples, where each sample consists of expert-segmented multiple structures. We estimate the joint shape density  $P(\tilde{\mathbf{C}})$  through kernel density estimation:

$$P(\tilde{\mathbf{C}}) = \frac{1}{N} \sum_{i=1}^N \prod_{j=1}^m k(d(\phi_{\tilde{C}_i^j}, \phi_{\tilde{C}_i^j}), \sigma_j). \quad (4)$$

We can then evaluate this density for any curve ensemble  $\tilde{\mathbf{C}}$ . Here  $k(\cdot, \sigma)$  is a Gaussian kernel with standard deviation  $\sigma$ ,  $\phi_C$  denotes the signed distance function of contour  $C$ , the index  $j$  refers to the  $j^{\text{th}}$  structure in the multi-structure ensemble, and  $i$  points to the  $i^{\text{th}}$  training sample. Finally,  $d(\cdot, \cdot)$  is a distance metric, and we use the Euclidean distance [3]. Given this learned density, its contribution to the gradient flow for (3) is given by (expressed for  $m = 2$  for simplicity):

$$\frac{\partial \phi_{\tilde{C}_i^j}}{\partial t} = \frac{1}{\sigma_j^2} \sum_{i=1}^N \lambda_i(\tilde{C}^1, \tilde{C}^2) (\phi_{\tilde{C}_i^j}(x, y) - \phi_{\tilde{C}_i^j}(x, y)) \quad (5)$$

where  $j = 1, 2$ ,  $\lambda_i(\tilde{C}^1, \tilde{C}^2) = \frac{k_i^1 k_i^2}{N \cdot P(\tilde{C}^1, \tilde{C}^2)}$ , and

$k_i^j = k(d(\phi_{\tilde{C}_i^j}, \phi_{\tilde{C}_i^j}), \sigma_j)$ . Note that training shapes that are closer to the evolving contour influence the evolution with higher weights. Note also that the weighting function  $\lambda_i(\tilde{C}^1, \tilde{C}^2)$  exhibits the coupling between the multiple structures.

## 2.2 Relative Pose Prior for Multiple Structures

In this subsection we discuss the learning and use of  $P(\bar{\mathbf{C}}|\tilde{\mathbf{C}})$ . We estimate  $P(\bar{\mathbf{C}}|\tilde{\mathbf{C}})$  through kernel density estimation as follows:

$$P(\bar{\mathbf{C}}|\tilde{\mathbf{C}}) = \frac{1}{N} \sum_{i=1}^N \prod_{j=1}^m k(d(p_{int}^j, p_{int}^{j_i}), \sigma_j), \quad (6)$$

where  $p_{int}^{ji}$  is the relative pose of the  $i^{\text{th}}$  element of the  $j^{\text{th}}$  structure in the training set, whereas  $p_{int}^j$  is the relative pose of the  $j^{\text{th}}$  structure in the candidate curve ensemble. Here  $d(\cdot, \cdot)$  is a weighted Euclidean distance. In 2D (for notational simplicity and without loss of generality), the relative pose of each structure is given by  $p_{int} = [A, c_x, c_y, \theta]$ .<sup>2</sup> Here,  $A$  is the area,  $c_x$  and  $c_y$  are the coordinates of the structure, and  $\theta$  is the orientation of the structure, all computed after global alignment.

We use moments to compute the relative poses:  $p_{int} = [m_{0,0}, \frac{m_{1,0}}{m_{0,0}}, \frac{m_{0,1}}{m_{0,0}}, \theta]$ . Here,  $m_{0,0}$  represents area,  $\frac{m_{1,0}}{m_{0,0}}, \frac{m_{0,1}}{m_{0,0}}$  are horizontal and vertical positions relative to the mass center, and  $\theta$  is the orientation. Following [5], the two-dimensional moment,  $m$ , of order  $p + q$ , on a signed distance function  $\phi$ , is computed as:  $m_{p,q} = \int_{x=-\infty}^{\infty} \int_{y=-\infty}^{\infty} x^p y^q H(-\phi(x, y)) dx dy$ , where  $H$  is the heaviside function. The orientation of contour  $C$  is defined as [5]

$$\theta(C) = \frac{1}{2} \arctan \left( \frac{2(m_{1,0}m_{0,1} - m_{1,1}m_{0,0})}{(m_{0,2} - m_{2,0})m_{0,0} + m_{1,0}^2 - m_{0,1}^2} \right)$$

Let  $k_i^j = k(d(p_{int}^j, p_{int}^{ji}), \sigma_j)$ . Then, the gradient flow for (6) is

$$\frac{\partial \phi_{\bar{C}^j}}{\partial t} = \frac{1}{P(\bar{C}|\tilde{C}) \cdot N} \sum_{i=1}^N \left( \prod_{j=1}^m k_i^j \right) \frac{MPF(j, i)}{\sigma_j^2} \delta_\epsilon(\phi_{\bar{C}^j}), \quad (7)$$

where

$$\begin{aligned} MPF(j, i) &= (m_{0,0}^j - m_{0,0}^{ji}) \\ &+ \sum_{(r,s), r+s=1} \left( \frac{m_{r,s}^j}{m_{0,0}^j} - \frac{m_{r,s}^{ji}}{m_{0,0}^{ji}} \right) \frac{(x^r y^s m_{0,0}^j - m_{r,s}^j)}{(m_{0,0}^j)^2} \\ &+ (\theta^j - \theta^{ji}) \sum_{r=0}^2 \sum_{s=0}^{2-r} x^r y^s M_{rs}^{\theta_j} \end{aligned} \quad (8)$$

for each  $j \in \{1, \dots, m\}$ . In implementation, we employ  $\delta_\epsilon$ , which is a smooth approximation to  $\delta$  [1]. Here,  $m_{r,s}^j$  and  $m_{r,s}^{ji}$  denote the moments of  $\bar{C}^j$  and  $\bar{C}_i^j$ , respectively, and the angles  $\theta$  follow the same convention. Due to space limitations, we are not able to provide details about the term  $M_{r,s}^{\theta_j}$ , which can be found in [10].

Note that in order to specify the kernel size  $\sigma_j$  of the  $j$ th object, we use the maximum likelihood kernel size with leave-one-out method (see [7]). This choice is used both in Sections 2.1 and 2.2.

Overall, the contributions from the C&V data term [1], coupled shape prior (Eqn. (5)), and the inter-shape pose prior (Eqn. (7)) constitute the gradient flow for (3). These three forces are summed at each iteration of the segmentation process, after appropriate alignment operations [10].

### 3 Experimental Results

We present 2D and 3D experimental results for the head of Caudate Nucleus and Putamen of Basal Ganglia. In this context, we implemented the 2D and the 3D schemes employing different programming environment.

---

<sup>2</sup>We drop indices for simplicity.

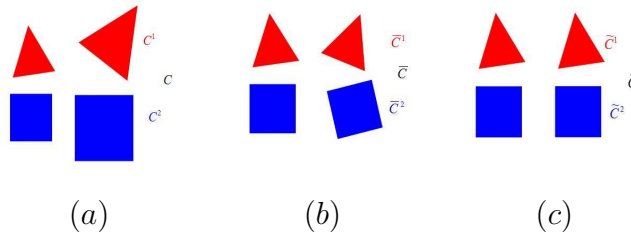


Figure 1: Alignment terms used for a multi-object that consists of a red triangle and a blue square. In each figure, the left side multi-object is a reference to which the right multi-object is aligned to. In Figure (a), the multi-object  $C$  is unaligned. In Figure (b),  $\bar{C}$  is aligned globally. In Figure (c),  $\tilde{C}$  is aligned locally, i.e. each (sub)object is aligned separately. In Figures (b) and (c), the multi-objects are not superimposed due to illustration reasons.

In our experiments, we demonstrate the effects of coupled shape and inter-shape pose prior in comparison with C&V and the single shape prior [3] based segmentations. In all the experiments, we use the same data term in each method. The usage of the same data term simplifies the comparison of our approach with others since only the coupled shape or inter-shape pose prior components of the methods are different.

Our ground truths are binary images which are created by medical operators who manually segmented the Caudate Nucleus and the Putamen of real brain MR images. For manual segmentation, we designed and implemented user guided interfaces following our medical operators' requirements.

### 3.1 Experiments on 2D data

We implemented the 2D scheme using C++ and Matlab. We built dynamic linked libraries in C++ that are called from Matlab. The Matlab environment was used for visualization.

In this section, we show and compare results of segmentation on real MR data. We present results on T2 and proton density (PD) MR images. Especially PD modality presents challenges due to its low contrast. We show the results using C&V, single shape prior, coupled shape prior, and inter-shape pose prior. In these experiments, we also analyze several segmentation results of using coupled shape and inter-shape pose priors both separately and together. We demonstrate the effects of coupled shape and inter-shape pose prior in comparison with the C&V force (see [1]) and the single shape prior (see [3]) based segmentations.

We compare the segmentations of the complete head of Caudate Nucleus and Putamen using three methods. We demonstrate the results of this experiment in Figure 2. Each method starts with the same initial conditions and we show the results obtained in steady state. We use a training set of twenty binary shapes that include the structures of interest. The C&V method with curve length penalty, alone, results in inevitable leakages for both Caudate Nucleus and Putamen (see first column). In the second and third column, we show the results obtained using single shape prior for separate structures. For the head of Caudate Nucleus, the single shape prior method presents significant missing and small leakages towards the Ventricles. For Putamen, all the segmentation results present lateral leakages. However, the proposed coupled shape prior based approach segments both structures more effectively due to the coupling effect between shapes (see the fourth column in Figure 2). We observe that the coupled shape force recovers the missed regions of Caudate Nucleus

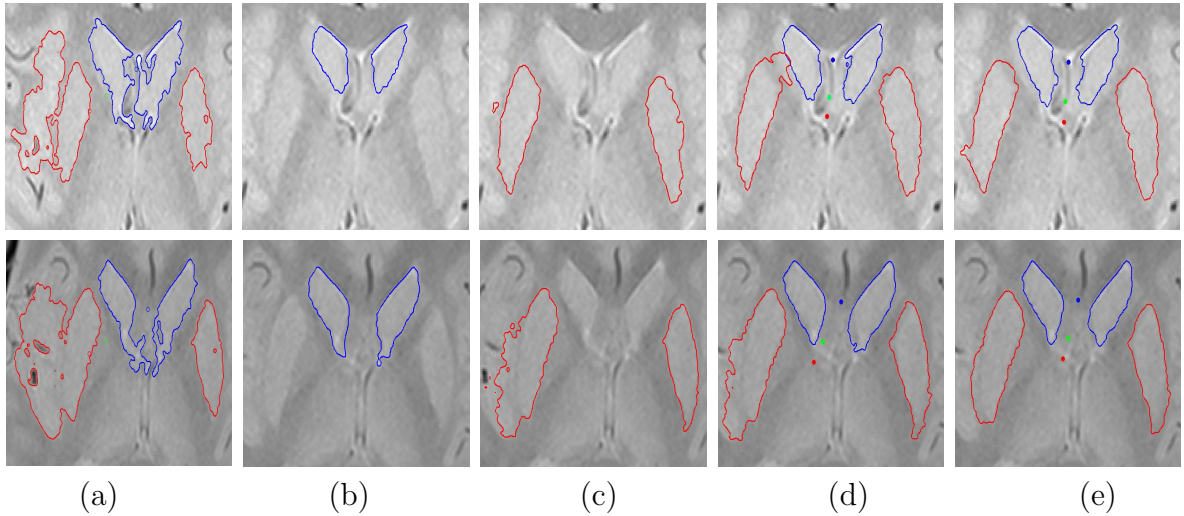


Figure 2: Segmentation results of the Caudate Nucleus and the Putamen in an MR slice: (a) C&V method with curve length penalty, (b) and (c) single shape prior for separate structures Caudate Nucleus and Putamen, (d) proposed coupled shape prior only, (e) proposed coupled shape and inter-shape pose prior. The top three lines is PD modality, while the bottom is T2.

and provides better accuracy in segmenting the Putamen, as compared to the single shape prior method. The benefit of using a coupled prior is expected to be greater when the boundary of some objects is not well supported by the observed image intensity (see Putamen results in the fourth and the fifth rows, which are T2 MR modalities). When applying the synergy between the coupled shape and the inter-shape pose forces we reduce the overall error in Caudate Nucleus and Putamen for all images. This result is shown in Figure 2 (see fifth column). In these series of experiments, we observe that coupled shape and inter-shape pose priors provide much more structured shape and strong geometry constraints on objects. In particular, the size and the distance constraints between shape pairs, improve the accuracy results significantly.

### 3.2 Experiments on 3D Real Data

For implementing evolving surfaces, we chose the level set framework of the ITK library, (see <http://www.itk.org/>). We inherited the `SegmentationLevelSetImageFilter` and the `SegmentationLevelSetFunction` classes from the `itk` namespaces. We create a filter object for each structure we want to segment, for example one for Caudate Nucleus and another one for the Putamen. (Note that, in this context, we use the term filter following the ITK terminology.) In each iteration of the multi-structure segmentation scheme, each filter runs its update function one step. When all the filters executed one step, a cross-filter operation is executed. In this cross-filter operation, Equations (4) and (6) are evaluated.

We also use the ITK library for reading data, resampling, as well as ground truth geometric processing. In this context, we built an editor of ground truths, (see Section 3.3 and Figure 6). The VTK library (see <http://www.vtk.org/>) is used for visualization purposes.

The bottleneck of the time processing is registration, however. Therefore, we used a fast registration technique, based on moments (see [2]). Figure 3 illustrates the results of registration of

two multi-structure objects. Each object consists of a Caudate Nucleus and a Putamen. When applying [2], we report that the relative difference of masses of any two registered medical objects is less than 5%. Our scheme requires about one hundred seconds to reach the steady state for each 200x200x50 voxel volume.

We built a database of seven T2 MR images, courtesy of Yeditepe hospital, and registered all these images. We show the results of the segmentations of C&V, the shape prior, and the synergy of shape prior and inter-shape prior based methods in Figures 4, and 5. We show a comparison among the segmentation results of the three methods, using super-positions of transparent surfaces in Figure 4. We present the complete combined result of the multi-structure segmentation in Figure 5. In all the images, we show that when applying C&V there are serious leakages, for example, in Figures 5 (c) and (d), the left and right Caudate Nucleus overlap. Unlike this, when applying coupled shape priors and inter-shape based priors, the left and right Caudate Nucleus structures are separate, see, for example, Figures 5 (e), (f), (g), and (h). We achieve better overall accuracy, i.e. smaller Dice coefficients, when applying our method as compared to existing techniques.

### 3.3 3D Ground Truth Editor

An important tool that we have built is an editor of ground truths, a snapshot is depicted in Figure 6. This editor is able to read data in DICOM and Analyze formats. The editor uses multi modality interaction options. The editing is performed via contours that are implemented using `vtkSplineWidget` class. A saving module performs reconstruction of the volume marked by the contours.

## 4 Conclusion

In this paper, we have proposed a multi-object segmentation approach that employs coupled shape and inter-shape pose prior information of different Basal Ganglia structures. We employ an active contour framework towards evolving different contours in parallel. We employ training based priors to estimate the coupled shape information as well as the inter-shape pose information among structures of interest. The priors are modeled using Parzen density estimation. We have demonstrated our approach in several experiments, in which poorly contrasted difficult shapes are segmented. We have also experimentally shown our scheme’s capabilities of occlusion recovery.

## Acknowledgment

The MR brain data sets were provided by the Radiology Center at Anadolu Medical Center and Yeditepe University Hospital. We also would like to thank Zeynep Firat, who is a radiologist at Yeditepe University Hospital, for providing manual segmentation of Basal Ganglia structures for validation.

## References

- [1] Tony F. Chan and Luminita A. Vese. Active contours without edges. *IEEE Transactions on Image Processing*, 10(2):266–277, 2001.
- [2] Tracy L. Faber and Ernest M. Stokely. Orientation of 3-d structures in medical images. *IEEE Transactions on Pattern Analysis and Machine Intelligence*, 10(5):626–633, 1998.
- [3] Junmo Kim, Müjdat Çetin, and Alan S. Willsky. Nonparametric shape priors for active contour-based image segmentation. *Signal Processing*, 87(12):3021–3044, December 2007.
- [4] Erik Madsen and Jonathan D. Gitlin. Copper and iron disorders of the brain. *Annual Review of Neuroscience*, 30:317–337, March 2007.
- [5] Richard J. Prokop and Anthony P. Reeves. A survey of moment-based techniques for unoccluded object representation and recognition. *CVGIP: Graphical Models and Image Processing*, 54(5):438–460, September 1992.
- [6] Torsten Rohlfing, Daniel B. Russakoff, and Calvin R. Maurer Jr. Performance-based classifier combination in atlas-based image segmentation using expectation-maximization parameter estimation. *IEEE Transactions on Medical Imaging*, 23(8):983–994, 2004.
- [7] Bernard W. Silverman. *Density Estimation for Statistics and Data Analysis*. Chapman Hall/CRC, London, 1986.
- [8] Andy Tsai, Anthony J. Yezzi, and Alan S. Willsky. A curve evolution approach to medical image magnification via the Mumford-Shah functional. *Medical Image Computing and Computer-Assisted Intervention, Lecture Notes in Computer Science*, 1935:246–255, 2000.
- [9] Gökhan Uzunbaş, Müjdat Çetin, Gözde Ünal, and Aytül Erçil. Coupled nonparametric shape priors for segmentation of multiple basal ganglia structures. *The Fifth IEEE International Symposium on Biomedical Imaging: From Nano to Macro, ISBI 2008.*, pages 217–220, 2008.
- [10] Mustafa Gökhan Uzunbaş. Segmentation of multiple brain structures using coupled nonparametric shape priors. *M. Sc. Thesis, Sabanci University*, 2008.

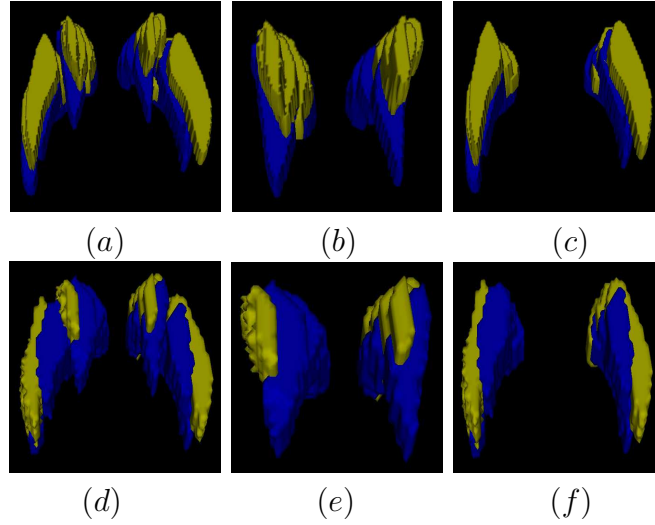


Figure 3: Registration of two multi-structure objects. Each multi-structure object consists of a Caudate Nucleus and a Putamen. Figure (a) represents two unregistered multi-structure objects. Figures (b) and (c) represent the Caudate Nucleus and the Putamen parts of the objects in (a). Figure (d) represents the registration result of the objects in (a). (e) and (f) represent the Caudate Nucleus and the Putamen parts of the objects in (d).

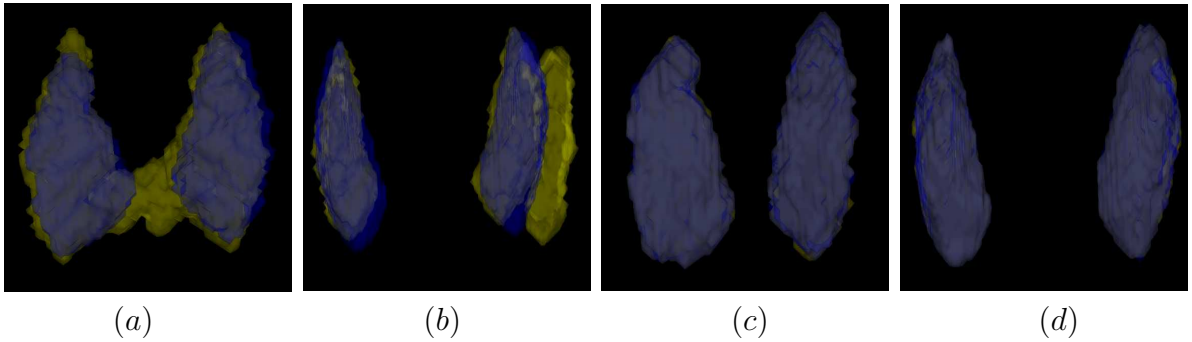


Figure 4: Comparison of segmentation results. Figures (a) and (c) represent Caudate Nucleus segmentation results. Figures (b) and (d) show Putamen segmentation results. Figures (a) and (b) represent a comparison between the result achieved using C&V with the one obtained using shape prior methods. While the segmentation result of *C&V* is shown in green, the shape prior method's result is shown in blue. Figures (c) and (d) represents a comparison between the result achieved using the shape prior method with the one obtained by employing the shape the inter-shape pose prior methods. The segmentation result of the shape prior based method is shown in green, while the synergy of the two methods is shown in blue.

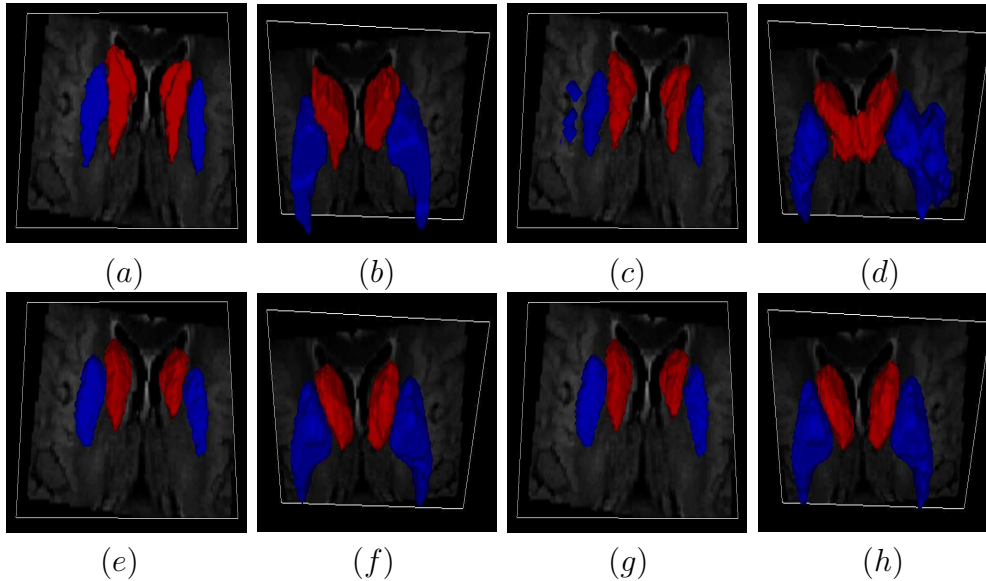


Figure 5: A result of 3D segmentation of a multi-structure object using our method. The red and blue structures represent Caudate Nucleus and Putamen, respectively. Odd and even columns illustrate views from an upper and an under point (as related to the volume of interest), respectively. In this context, the volume is rotated horizontally (as related to the viewer position) from odd to even and adjusted. The adjustment aims keeping the Ventricles as a reference. Figures (a) and (b) show ground truths. Figures (c) and (d) show the volumetric segmentation result of C&V. Figures (c) and (d) show severe leakages that occur in the Caudate Nucleus and the Putamen segmentation respectively. Figures (e) and (f) show the segmentation result when using shape prior. Figures (g), and (h) show the segmentation result when using shape the inter-shape pose prior.

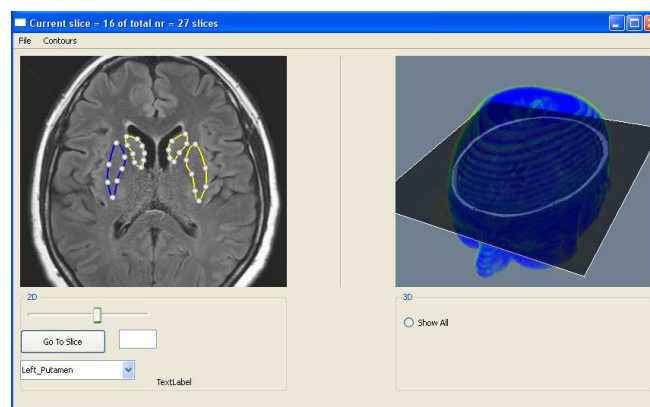


Figure 6: 3D ground truth editor. The left part is a 2D sectioning plane. This plane is superimposed to the volumetric data in the right part of the editor window, in order to provide the medical operator cues about the 3D positioning. Several other indicators are also provided, for example the number of the slice in the processed set, as can be seen in the upper part of the window.